International Journal of Nanoelectronics and Materials
IJNeaM
ISSN 1985-5761 | E-ISSN 2232-1535

Study based on micro- and nanosized raw materials using the hydrothermal method

Roaa Abbas [a], Evan Salim [b]*, and Rana Mahdi [b]

[a] *Ministry of Science and technology, Baghdad, Iraq*
[b] *Applied science department, University of Technology-Iraq*
** Corresponding author. e-mail: evan_tarq@yahoo.com evan.t.salim@uotechnology.edu.iq*

Received 24 January 2024, Revised 25 August 2024, Accepted 7 September 2024

ABSTRACT

The hydrothermal approach has been applied to the synthesis of cuprous oxide on a quartz substrate. For 12 hours at 100°C, different morphologies of micro (50 µm) and nano (30 nm) copper powder were examined at a concentration of roughly 0.1 g. Using a scanning electron microscope (SEM), spherical and dendritic-like structures were formed for nano and micro particle sizes, respectively. The presence of cuprous oxide was demonstrated by X-ray analysis, and under the aforementioned circumstances, UV-VIS spectroscopy was utilized to identify the characteristics of the absorption band and band gap energy of cuprous oxide synthesis. The AFM method was used to study the surface topography for nano and micro particle sizes. The composition of the prepared sample was examined using FTIR. A DC measurement was utilized to investigate the electrical characteristics.

Keywords: *Hydrothermal, Copper powder, Cuprous oxide, Spherical, Dendrite-like structure.*

1. INTRODUCTION

Cuprous oxide (Cu_2O) is a p-type semiconductor with a direct band gap of about 2.17 eV and a reddish color. Cuprous oxide crystals are highly significant due to their uniform and controllable morphology, as well as their optimized synthesis for various applications, owing to their optical, magnetic, and electrical properties [1]. Cuprous oxide is an intriguing material with a wide range of applications. Among the various materials found in the Earth's crust, Cu_2O stands out as unparalleled, low-cost, non-toxic, abundant, and environmentally friendly. Consequently, it has been extensively utilized in numerous applications and research areas [2, 3]. Various methods have been employed for the synthesis of cuprous oxide [4]. In 2002, Borgohain et al. [5] used an electrochemical method for Cu_2O synthesis. Other techniques include laser ablation [6], sol-gel [7], heat treatment [8], magnetron sputtering [9], chemical spray pyrolysis [10], and the hydrothermal method (HTM). The HTM involves a formation mechanism where crystals are obtained through reactions in water at specific temperatures and pressures [11].

With the increasing demand for advancements in material science, the hydrothermal method has emerged as a promising new technology for preparing thin films. This chemical synthesis technique has rapidly developed in recent years, enabling the creation of innovative materials and composites [12].

In a previous study [13], Cu_2O with three distinct branching morphologies was synthesized using the hydrothermal method with copper acetate and sodium tartrate at varying concentrations and temperatures. Additionally, open-hollow nanostructured Cu_2O was successfully prepared through the same technique. The temperature and Cetyltrimethylammonium Ammonium Bromide (CTAB) of the detergent have an interesting role in preparing the cuprous oxide (Cu_2O) at 120°C for 24 h [14]. First, the hydrothermal method was employed to synthesize cuprous oxide (Cu_2O) with a nanoflower-like structure, approximately 230 nm in size. Copper acetate monohydrate was used as the copper source, with glucose, at 140°C for 6 hours [15]. The flower-like structure of Cu_2O was obtained in distilled water at temperatures ranging from 50 to 200°C. This resulted in the development of a relatively simple and inexpensive method for fabricating Cu_2O with a flower-like structure [16]. A straightforward hydrothermal synthesis of copper oxide was reported, with the final results showing that the hydrothermal method (HTM) is significantly influenced by the process time, detergent concentration, and temperature [17].

The hydrothermal method was employed to create micro-sized cuprous oxide using $CuCl_2$, NaOH solution, ascorbic acid (AH_2) as the reductant, and CTAB. The resulting product was six-cornered truncated octahedra, which were obtained by increasing the molar ratio of NaOH to $CuCl_2$ [18]. Additionally, rose-like Cu_2O nanoflowers were synthesized using the hydrothermal method with CTAB. This approach was chosen to leverage the effects of CTAB on the morphology of the nanoflowers and to enhance their suitability for specific applications [19]. The aim of this research is to develop a novel hydrothermal method, incorporating layer-by-layer deposition, to create cuprous

oxide with various morphologies. This method combines deionized water, micro- and nano-sized copper powders, and heating the mixture to approximately 100°C, eliminating the need for special reagents. This approach aims to reduce costs and simplify fabrication for a range of applications.

2. EXPERIMENTAL SECTION

Optimization of the synthesis process was the prime target of this study. 0.1 g of copper, with different grain sizes, was mixed with deionized water of about 40 mL using a magnetic stirring for one hour to obtain a homogeneous precursor solution. After this period of time, the solution was transferred to an autoclave lined with Teflon cells at a temperature of about 100°C for the synthesis of Cu_2O, layer by layer. The first layer took 6 hours to form. The system was then turned off and allowed to cool to room temperature, followed by drying the film at temperatures below 70°C. After one hour of stirring, the formation of the second layer began, and the same procedure was repeated to complete a total of 12 hours for the Cu_2O thin film. The characteristics of the prepared thin film were evaluated using X-ray diffraction (LabX XRD-6000) and UV-Vis spectroscopy (Metertech SP8001 spectrophotometer). To assess the optical, structural, and compositional properties of the synthesized sample, a field emission scanning electron microscope (Inspect F50) operated at 30.0 kV was employed. Atomic force microscopy (AFM) was conducted using the AFM TT-2 (AFM Workshop, USA), while the electrical characteristics of the prepared samples were measured with a Keithley electrometer. Additionally, the characteristics of the thin films were analyzed using Fourier transform infrared spectroscopy (FTIR Spectrum Two, PerkinElmer, USA).

3. RESULT AND DISSCUSION

3.1. X-Ray

The structural properties and particle size of the synthesized Cu_2O were investigated using X-ray diffraction. The X-ray diffraction results plot the intensity of the signal against various diffraction angles, measured at their respective 2θ positions. These 2θ positions correspond to specific spacings between crystals or atoms in the sample [20], determined by the angle of diffraction from the incident X-ray beam interacting with the sample. The intensity of the peaks is indicative of the quantity of molecules or crystals with that particular spacing [21]. A higher peak intensity signifies a greater quantity of crystals or molecules with the same spacing. The typical X-ray diffraction pattern of the synthesized Cu_2O is shown in Figure 1.

Figure 1 displays the emission peaks for copper nano powder. The diffraction peaks are observed at approximately 2θ values of 36.3°, 42.2°, 61.3°, and 73.6°, corresponding to the (111), (200), (220), and (311) planes, respectively.

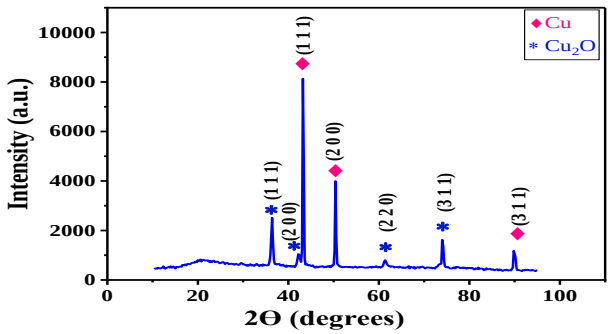

Figure 1. X-Ray for copper nano powder using in hydrothermal technique to obtain Cu2O.

These peaks are attributed to the presence of Cu_2O, with d-spacings of 2.4, 2.1, 1.5, and 1.2 Å, and confirm a cubic structure, as indicated by the standard JCPDS file no. 99-0041. Therefore, the growth rate of the crystals of Cu_2O increases progressively along the directions of these planes. The 2θ values at 43.2°, 50.4°, and 89.9° correspond to the (111), (200), and (311) planes, respectively, indicating the presence of copper with d-spacings of 2.0, 1.8, and 1.0 Å. The position and intensity of these peaks align well with the values reported in the reference code 03-065-3288. The crystal size for Cu_2O was estimated to be approximately 13.4 nm, determined using the Scherrer equation [22]:

$$D = K\lambda/\beta\ cos\theta \quad (1)$$

where, K is the Scherrer constant, which ranges from 0.68 to 2.08 depending on the particle shape, with a typical value of 0.94 for spherical particles with cubic symmetry. β represents the full width at half maximum (FWHM), λ is the wavelength of the X-ray, which is 1.54 Å for CuKα radiation, and θ is the diffraction angle obtained from the X-ray measurement [23].

When crystals are formed at 100°C for 12 hours, the preferential adsorption reduces the surface energy of the bound planes and inhibits crystal growth perpendicular to these planes [24]. Figure 2 displays the X-ray diffraction analysis of copper micro powder, with diffraction peaks appearing at 22.1°, 38.0°, 43.4°, 50.4°, 61.3°, and 73.7°. The crystal size, determined using the Scherrer equation, was approximately 23.4 nm.

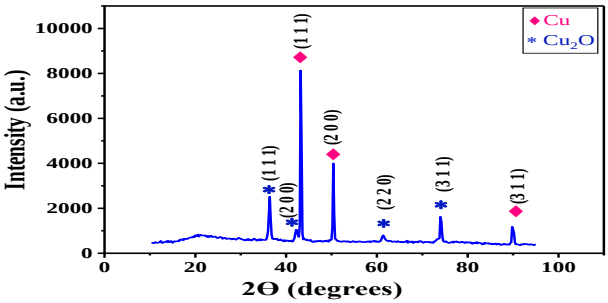

Figure 2. X-Ray for copper micro powder

Figure 2 also shows the X-ray diffraction analysis for copper micro powder. The diffraction peaks at 22.1° and 38° correspond to CuO, with d-spacings of 4.0 and 2.4. The

peaks at 61.3° and 73.7° are attributed to Cu_2O, with d-spacings of 1.5 and 1.2. Additionally, the peaks at 43.4° and 50.4° are associated with copper powder, with d-spacings of 2.0 and 1.8.

The broadening in the peak can be attributed to the atomic position change which resulted from strain [25]. In another study, it was reported that as particle size increases, the full width at half maximum (FWHM) decreases. Thus, the overall peak broadening results from a combination of strain and particle size effects. For nanoparticles, the particle size determined using the Scherrer equation is smaller than that for microparticles, resulting in narrower peak broadening compared to micro powders [26]. Williamson Hall studied the reason behind the width of the peak, and he attributed that to the strain, as elucidated in Figure 3 a, b.

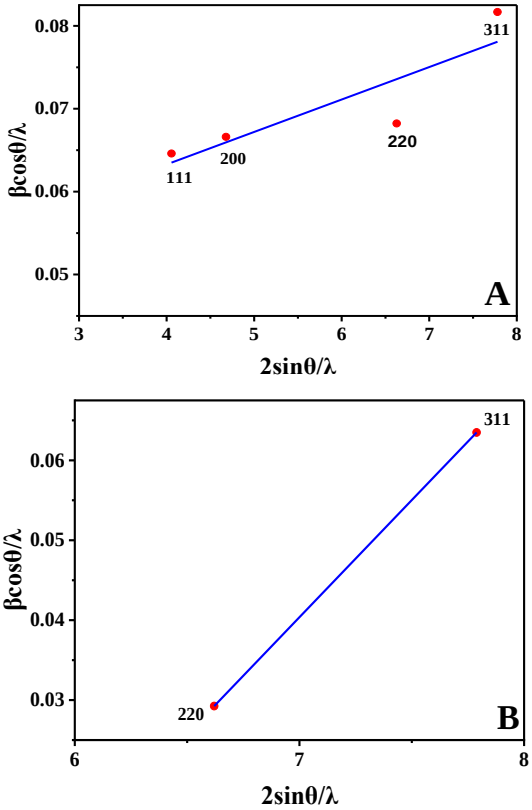

Figure 3. Effect of the strain and particle size on the broad: (A) for nano powder (B) for micro powder.

where βcosθ/λ was plotted with respect to 2sinθ/λ for the peaks of copper powder which was used for the formation of cuprous oxide. Particle size and strain are determined from the y-axis intercept and the slope of the fitted line. Strain might have occurred due to lattice shrinkage, as indicated by the lattice parameter calculations. The y-axis intercept of the straight line represents the reciprocal of the crystal size. As shown in Figure 3, the crystal size is approximately 21 nm for nanoparticles and 34.2 nm for microparticles, which is consistent with the results obtained from the Scherrer equation [27].

3.2. Scanning Electron Microscope (SEM)

In the hydrothermal method, copper powder was initially used as the precursor for synthesizing cuprous oxide. Cu_2O crystals grew randomly at a low hydrothermal temperature (approximately 100°C) on a quartz substrate over 12 hours, resulting in spherical nanoparticles, as shown in Figure 4. The morphology of the products is highly dependent on temperature, time, and other parameters of the hydrothermal treatment during the synthesis [28].

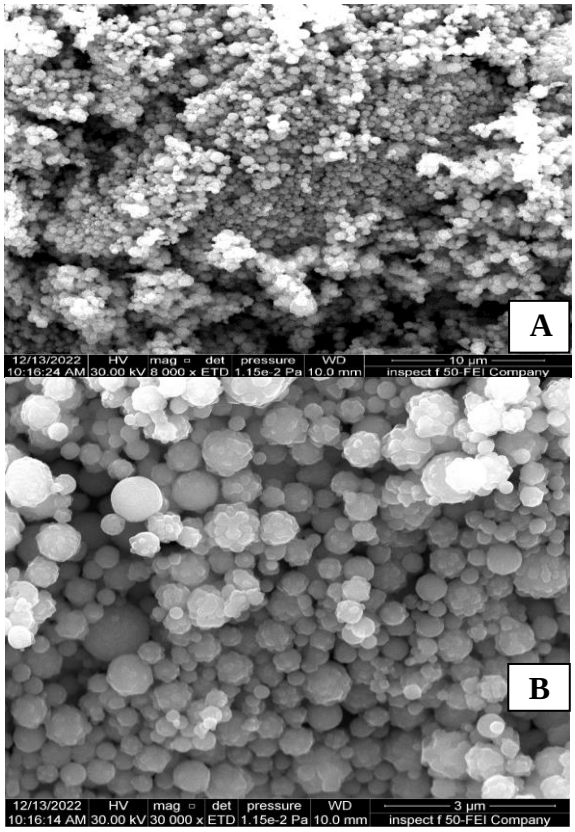

Figure 4. SEM image for copper nano powder at different scales (A) at 10µm (B) at 3µm.

Spherical nanoparticles of Cu_2O accumulated to form polycrystalline structures with a rough external surface. As particles accumulated layer by layer on the quartz substrate, effective nucleation increased the thickness of the thin film. In cuprous oxide (Cu_2O), the amount of copper (Cu+) is approximately twice that of oxygen (O2-). The crystal lattice varies across different planes, with different surface atom arrangements: the (100) plane represents a polar surface, while the (111) plane is nonpolar. During the formation of cuprous oxide, nuclei were formed, and the desorption and adsorption of ions on different Cu_2O planes influenced the crystal growth direction and the shape of the resulting particles [29]. Figure 5 shows the EDX and the exploited area with different colors for the thin film of copper nano powder. As shown in Figure 5, the presence of silicon can be attributed to the quartz substrate, which contributes to the undeveloped space in the sample.

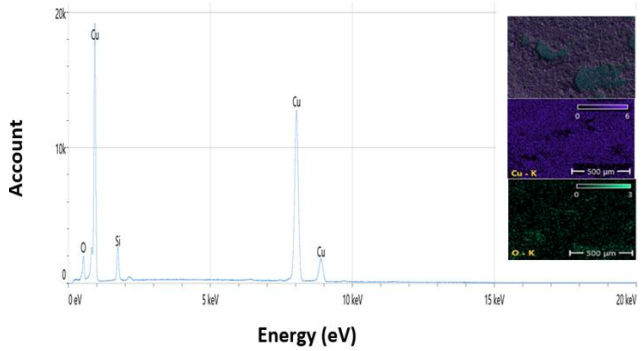

Figure 5. EDS for copper nano powder with the map plot.

Furthermore, Figure 5 shows a map plot where green indicates the presence of oxygen in the sample, and purple represents copper. The amount of oxygen is lower than copper, which aligns with the formation of cuprous oxide where two copper atoms are paired with one oxygen atom. This explains the presence of copper nanoparticles observed in the XRD analysis. For the copper micro powder, the hydrothermal synthesis produced a dendrite-like structure, as shown in Figure 6.

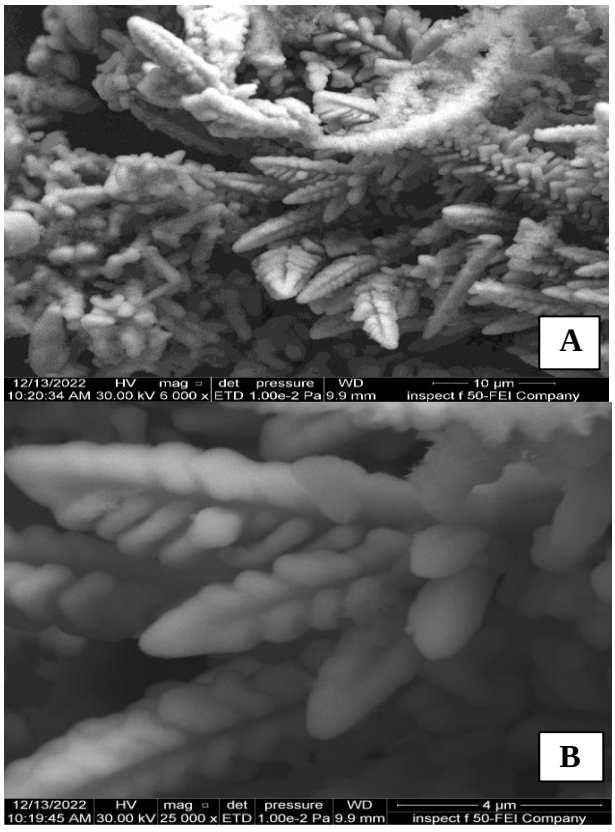

Figure 6. SEM image for copper micro powder(a)at 10µm (b) at 4µm.

Controlling the shapes of crystals is highly interesting due to various factors, such as bonding, surface energy, and electronic structure, which are strongly related to the resulting morphology [30].

The behavior of dendrite-like Cu_2O crystal growth indicates that dendrites form in a stirred electrolyte, while octahedral structures are observed in a static electrolyte. The morphological properties are influenced by the transfer of Cu_2+ ions. The depletion area around the Cu2+ nuclei is disrupted, and under hydrothermal conditions, a face-centered cubic (FCC) Cu lattice forms due to the deposition of Cu_2+ ions. The lattice expansion corresponds to the formation of a cuprite Cu_2O lattice, where oxygen atoms diffuse into the copper lattice. As a result, the structure of the cuprous oxide (Cu_2O) crystal enhances the dendritic-like structure and influences the growth direction of the dendritic branches [31]. With less nucleation on the substrate surface, the thickness of the thin film is lower compared to that of the nano powder. The particles accumulated on the substrate, leading to a reduced presence of copper relative to the oxide. Figure 7 illustrates the particle aggregation, and the map shows regions of oxygen, copper, and silicon. The high concentration of silicon is likely due to the quartz substrate, which contributes to the low film thickness and reduced growth rate on the substrate.

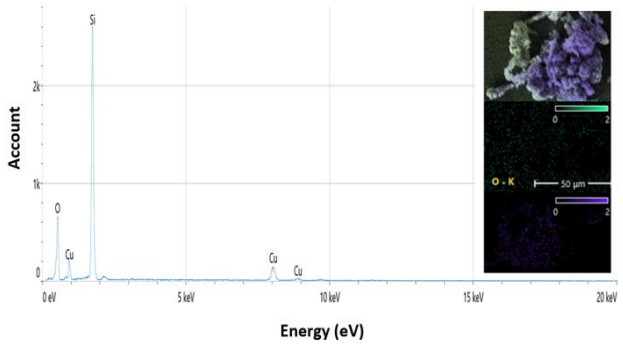

Figure 7. EDS for copper micro powder with the map plot.

3.3. UV-VIS Spectroscopy

The optical properties and band gaps of the prepared samples are obtained from a UV-VIS spectrophotometer [32]. The UV-VIS spectrum reveals a transmittance peak for the spherical-like cuprous oxides (Cu_2O) prepared using copper nano powder, as shown in Figure 8.

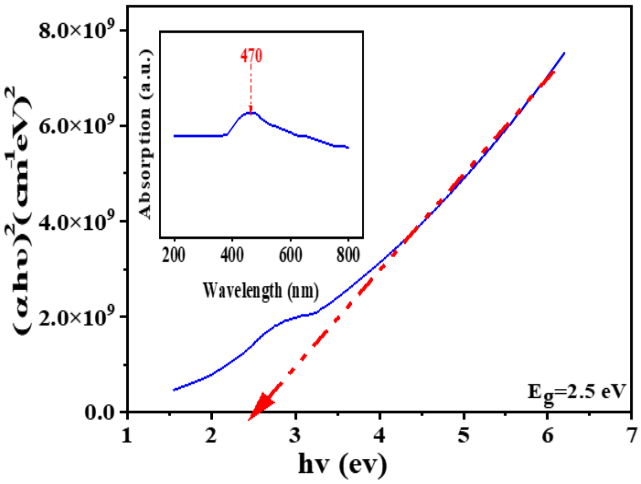

Figure 8. UV-VIS for copper nano powder

The absorption peak for copper nano powder appears at 470 nm. This band is attributed to the band-to-band transition of the Cu-oxide nanocrystals suspended in water. It may also be related to the small particle size and the associated energy gap [33]. The transition peak for the

dendrite-like structure of copper micro powder is shown in Figure 9. The first peak at 456 nm is attributed to the presence of Cu_2O. Peaks at 727 nm are ascribed to the presence of $Cu/Cu_2O/CuO$ on the surface of the synthesized material. These peaks correspond to the formation of the CuO phase, as indicated by the XRD analysis [34]. Interestingly, this feature has been previously observed, where these bands progressively red-shift to the near-infrared (NIR) region as the nanomaterial diameters increase. The results suggest that this additional absorption feature is related to light scattering by larger Cu_2O nanoparticles, with dimensions on the order of hundreds of nanometers, similar to copper micro powder [35]. Figure 9 shows UV-VIS measurement for copper micro powder.

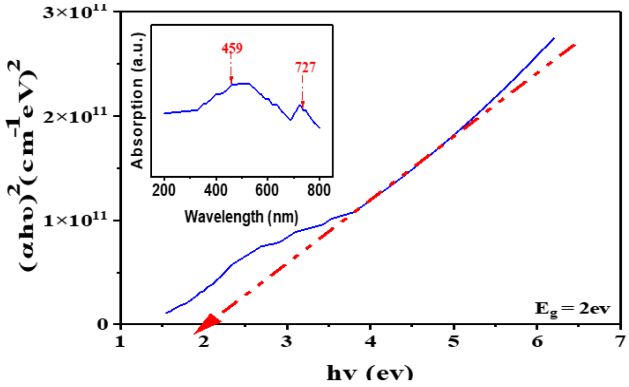

Figure 8. UV-VIS for copper micro powder.

The optical band gap value was calculated based on the electron transition from the valence band to the conduction band, which corresponds to the absorption peak. The relation between the absorbance coefficient (α) and the incident photon energy(hυ) is written as [36].

$$\alpha h\upsilon = A\,(h\upsilon - E_g)^n \qquad (2)$$

where, A is a constant, hυ is the photon energy, Eg is the energy gap, and n is the transition. The band gap estimated for the copper nano powder is about 2.5 eV, and the decrease in the particle size resulted in an increase in the band gap. The quantum confinement effect takes place when the particle size of nano-crystals decreases to become smaller than the Bohr radius of the electron-hole pair. On the other hand, for copper micro powder, the band gap is about (2 eV). As the wavelength increases, the band gap decreases, which indicates a reduction in the absorption peak and an increase in transmittance.

3.4. FTIR Measurement

FTIR measurement was conducted to study the compositional and chemical characteristics of the prepared Cu2O [37]. Figures 10 and 11 display the FTIR spectrum of the prepared samples for nano and micro copper powder, respectively, over the range of 400 to 4000 cm^{-1}.

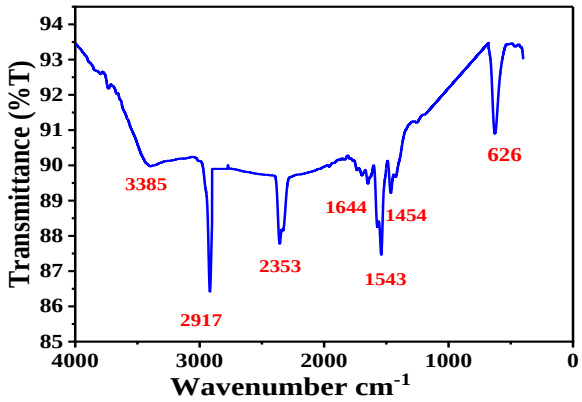

Figure 9. FTIR spectrum for copper nano powder.

The functional bond was observed at different positions, while the absorption band at 3385 cm^{-1} showed a symmetric or asymmetric stretching of O-H bonds, which might have been caused by the presence of water [38].
The vibrations peaks at 2917 cm^{-1} represent the presence of Cu_2O, while at 2353 cm^{-1} they were observed as a result of the presence of atmospheric CO_2 [39]. Metal-oxygen (Cu-O) bonds can be seen at 1644, 1543, 1454 cm^{-1}. The Cu_2O stretching bond can also be seen at 626 cm^{-1}, revealing the presence of a metal oxide group in the sample. This data is obtained in order to analyze the absorption level at each wavelength [40].

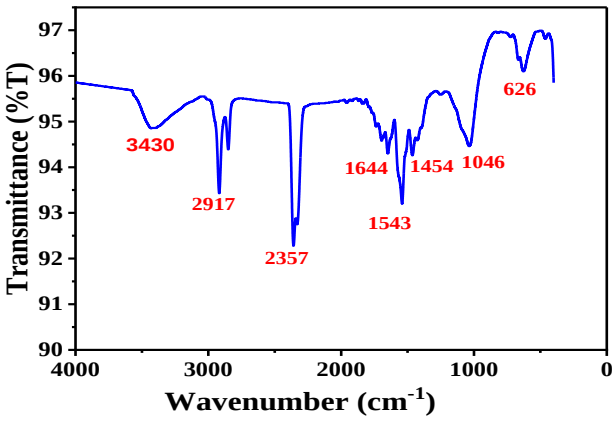

Figure 10. FTIR measurement for copper micro powder.

Most of the functional groups in Figure 11 display similar characteristics to those in nano copper powder, with some differences. Notably, the 3385 cm^{-1} bond is absent in the FTIR measurement for copper micro powder. Additionally, the absorption intensity increases for copper nano powder, indicating the presence of more specific bond numbers at particular wavenumbers. The peaks at 1046 and 3430 cm^{-1} are attributed to the presence of the CuO phase in the sample prepared using copper micro powder. This result supports the findings obtained from XRD.

3.5. Atomic Force Microscope (AFM)

This technique was employed for the investigation of surface morphology and consequently the effect of the formation technique on the quality of the thin film surface [41]. Topographical properties, such as average grain size, surface roughness, and root mean square (RMS) of the

samples of Cu_2O thin film deposition on a substrate were all investigated by atomic force microscopy (AFM).

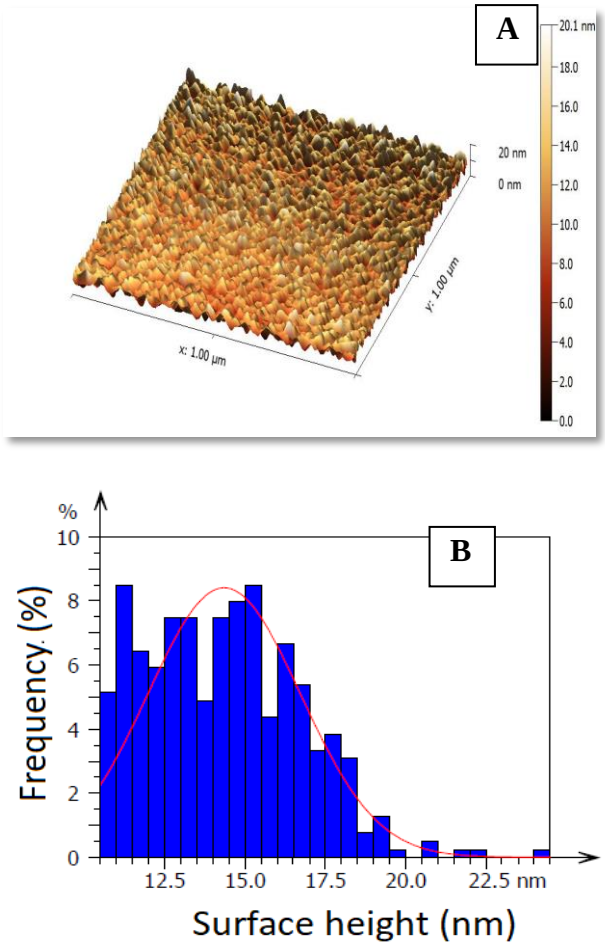

Figure 11. (A) AFM measurement for copper nano powder (B) histogram

Figure 12 elucidates the topography of the sample prepared by the hydrothermal method using copper nano powder at (100°C). The figure also shows that there is a bright and dark region which explains the difference in the roughness of the surface. The particle size of copper nano powder is smaller than copper micro powder, but the thickness of the thin film, which was measured using laser measurement, is found for copper nano powder to be about 190 nm, while for copper micro powder, it is about 158 nm. This may be due to the better nucleation of particles on the substrate. This suggests that one of the main advantages of hydrothermal methods is the ability to use particles as seeds, either in the form of thin films or nanoparticles, to direct the growth [42]. The root mean square (RMS) is defined as the square root of the distribution of surface height, and it is considered to be more sensitive than the average roughness for large deviations from the mean line/plane. The value of the root mean square for copper nano powder is about 3 nm, and for copper micro powder, it is about 6 nm. This can be attributed to the particle size. The roughness of the surface for copper micro powder is slightly less than for copper nano powder, as shown in Figure 13.

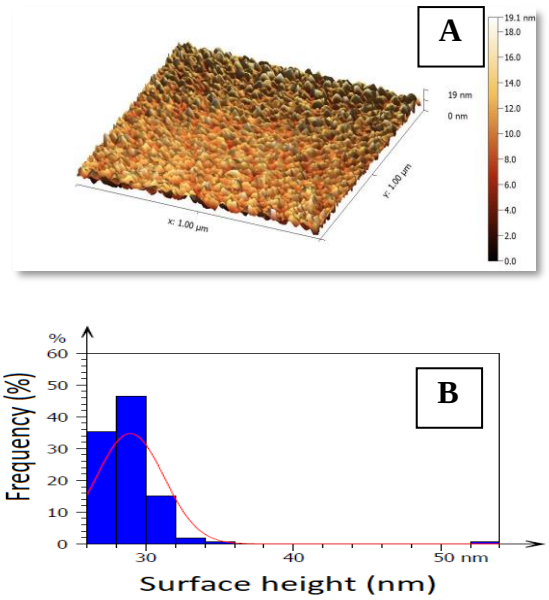

Figure 12. (A)AFM measurement for copper micro powder (B) histogram

The surface roughness for copper nano powder is about 2.3, while for copper micro powder, it is about 4.9. The increase in surface roughness for copper micro powder is due to the larger particle size compared to the copper nano powder. The grain size, as determined from AFM, was 14.5 nm for copper nano powder and 30 nm for copper micro powder, respectively.

3.6. Electrical characteristic and Figure of Merit

Similar to DC characteristics, the electrical characteristics of the film may support the thin film application [43]. In the DC measurement, the current passes through the sample via an electrode with a width of 1 cm, a spacing of about 3 mm between electrodes, and a film thickness of 190 nm for the copper nano powder and 158 nm for the copper micro powder. To clarify the electrical properties of the thin film prepared by the hydrothermal method using copper nano and micro powders, resistivity was measured as a function of temperature in the range of 40-150 °C, as shown in Figure 14.

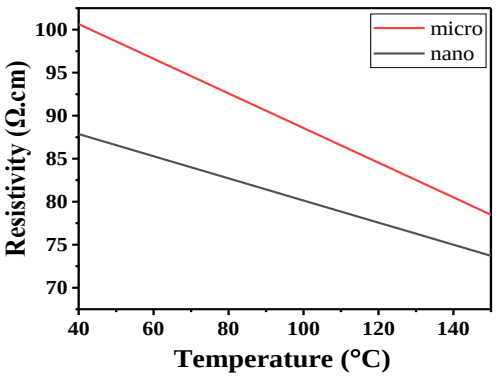

Figure 13. Electrical resistivity as a function of the temperature.

The resistivity of the prepared sample decreases as the temperature increases, indicating that conductivity improves with rising temperature due to the formation of semiconductor Cu_2O. The data in Figure 14 suggests that the sample exhibits typical semiconductor behavior, where an increasing number of thermally activated charge carriers can overcome the energy barrier and contribute to electrical conduction as the temperature rises. Notably, all known superconductors with critical temperatures above 40 K share a structure based on square-planar-coordinated Cu-O sheets. This fact has sparked significant interest in the behavior of carriers within Cu-O planes, which are believed to be responsible for superconductivity, as well as in the electronic interactions within simple copper oxides [3, 44, 45]. The conduction mechanisms were found to follow the well-known Arrhenius' equation:

$$\boldsymbol{\sigma = \sigma_0}\,(-E_a/K_bT) \qquad (3)$$

where, σ_0 is the pre-exponential factor, Ea is the activation energy of electrical conduction which corresponds to the minimum energy required for conduction from one site to another and undergoes physical transport, T is the absolute temperature, and KB is the Boltzmann constant. The activation energy (Ea) of the DC conductivity is calculated from the slopes of the two linear parts of the ln (□□□) versus 1/T plot, as shown in Figure 15.

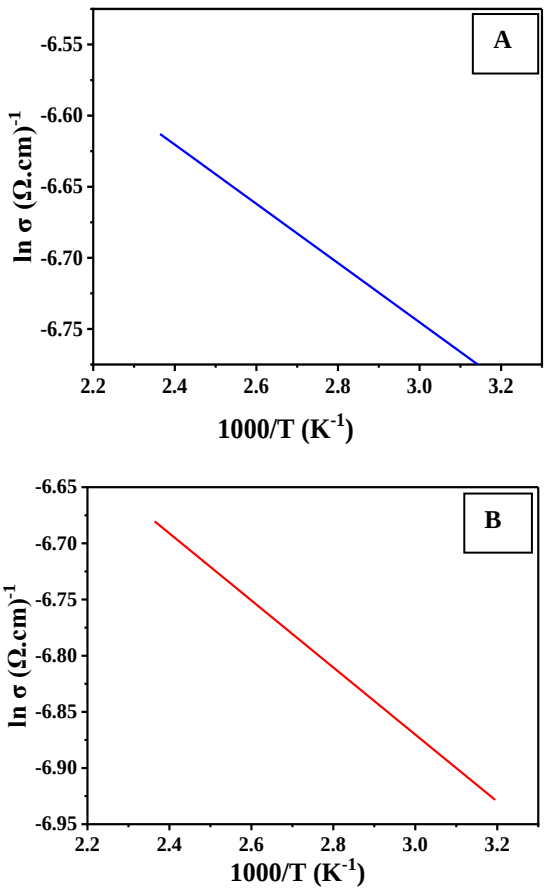

Figure 14. The electrical characteristic (a) activation energy from ln σ: for copper nano powder and (b) the activation energy from ln σ for copper micro powder.

The figure of merit was used to evaluate the performance of a method or system relative to its alternatives. This was done by determining the appropriate figure of merit for a specific application. To assess the suitability of the prepared films for optoelectronic devices, both electrical conductivity and visible light absorption were measured. These parameters are collectively known as the figure of merit (ϕ), which is estimated by applying the equation in [46]:

$$\phi = 1/\rho\, Ln(T_{ava}) \qquad (4)$$

where, ρ is the electrical resistivity measured based on the Dc measurement, and T is the transmittance average from 400-800 nm using UV-VIS measurement. The figure of merit for copper nano powder is about 0.0048, while for copper micro powder, it is about 0.0007. This indicates that copper nano powder is better than copper micro powder in many applications [47].

4. CONCLUSION

Copper nano and micro powders, using only deionized water, were employed to synthesize cuprous oxide via the hydrothermal method, with different particle sizes for each powder. X-ray diffraction (XRD) measurements revealed that monoclinic Cu_2O crystals were formed, with the copper nano powder producing particles around 13.4 nm in size, while the copper micro powder resulted in particles approximately 23.4 nm in size. SEM analysis revealed the presence of both spherical and dendrite-like cuprous oxide structures. Additionally, EDS indicated varying proportions of copper and oxygen in the copper nano powder, which explains the higher percentage of cuprous oxide observed in the X-ray measurement. In contrast, for the copper micro powder, the amount of copper was much lower than oxygen, resulting in a reduced presence of cuprous oxide in the X-ray measurement. The UV-VIS absorption peak further confirmed the existence of copper in the form of oxides. The UV-VIS spectroscopy measurement is in agreement with the quantum confinement effect (QCE). As the particle size decreases the energy gap increases. The band gap for copper nano powder is about 2.5 eV, and for copper micro powder, it is about 2 eV. FTIR measurements elucidated the chemical composition and bond presence on the film surface, indicating the presence of metal oxide and Cu_2O stretching bonds with high intensity for the copper nano powder. AFM analysis depicted the surface topography, showing a high nucleation rate for copper nano powder. The figure of merit measurement is a crucial factor in selecting the best material for a specific application, and the copper nano powder demonstrated a higher value.

ACKNOWLEDGMENTS

The authors would like to thank the University of Technology-Iraq for the logistic support of this work.

REFERENCES

[1] S. Sun, X. Zhang, Q. Yang, S. Liang, X. Zhang, and Z. Yang, "Cuprous oxide (Cu2O) crystals with tailored architectures: A comprehensive review on synthesis, fundamental properties, functional modifications and applications," *Progress in Materials Science*, vol. 96, pp. 111-173, 2018.

[2] A. Khan, M. Jawaid, and A. M. A. Asiri, *Nanocarbon and its composites: preparation, properties and applications*, Woodhead Publishing, 2018.

[3] A. S. Jasim and O. N. Salman, "The Effect of Solvent Variation on Structural, Optical, and Electrical Properties of TiO2 Films Prepared by Hydrothermal Method," *Journal of Applied Sciences and Nanotechnology*, vol. 3, no. 2, pp. 59-69, 2023.

[4] L. Yu, X. Y. Yu, and X. W. Lou, "The Design and Synthesis of Hollow Micro-/Nanostructures: Present and Future Trends," *Advanced Materials*, vol. 30, no. 38, 1800939, 2018.

[5] K. Borgohain, N. Murase, and S. Mahamuni, "Synthesis and properties of Cu2O quantum particles," *Journal of Applied Physics*, vol. 92, no. 3, pp. 1292-1297, 2002.

[6] K. Suzuki, N. Tanaka, A. Ando, and H. Takagi, "Size-selected copper oxide nanoparticles synthesized by laser ablation," *Journal of Nanoparticle Research*, vol. 14, pp. 1-11, 2012.

[7] L. Armelao, D. Barreca, M. Bertapelle, G. Bottaro, C. Sada, and E. Tondello, "A sol–gel approach to nanophasic copper oxide thin films," *Thin Solid Films*, vol. 442, no. 1-2, pp. 48-52, 2003.

[8] A. H. Jayatissa, K. Guo, and A. C. Jayasuriya, "Fabrication of cuprous and cupric oxide thin films by heat treatment," *Applied Surface Science*, vol. 255, no. 23, pp. 9474-9479, 2009.

[9] A. Ogwu, T. Darma, and E. Bouquerel, "Electrical resistivity of copper oxide thin films prepared by reactive magnetron sputtering," *Journal of Achievements in Materials and Manufacturing Engineering*, vol. 24, no. 1, pp. 172-177, 2007.

[10] D. Osorio-Rivera, G. Torres-Delgado, J. Márquez-Marín, R. Castanedo-Pérez, M. A. Aguilar-Frutis, and O. Zelaya-Ángel, "Cuprous oxide thin films obtained by spray-pyrolysis technique," *Journal of Materials Science: Materials in Electronics*, vol. 29, pp. 851-857, 2018.

[11] L. Y. Meng, B. Wang, M. G. Ma, and K. L. Lin, "The progress of microwave-assisted hydrothermal method in the synthesis of functional nanomaterials," *Materials Today Chemistry*, vol. 1, pp. 63-83, 2016.

[12] W. Choi, N. Choudhary, G. H. Han, J. Park, D. Akinwande, and Y. H. Lee, "Recent development of two-dimensional transition metal dichalcogenides and their applications," *Materials Today*, vol. 20, no. 3, pp. 116-130, 2017.

[13] X. L. Luo, M. J. Wang, D. S. Yang, J. Yang, and Y. S. Chen, "Hydrothermal synthesis of morphology controllable Cu2O and their catalysis in thermal decomposition of ammonium perchlorate," *Journal of Industrial and Engineering Chemistry*, vol. 32, pp. 313-318, 2015.

[14] S. Cao, T. Han, L. Peng, C. Zhao, and J. Wang, "Hydrothermal synthesis, characterization and gas sensing properties of novel Cu2O open hollow nanospheres," *Ceramics International*, vol. 43, no. 5, pp. 4721-4724, 2017.

[15] G. Aziz, "Hydrothermal synthesis of cuprous oxide nanoflowers and characterization of their optical properties," *Süleyman Demirel Üniversitesi Fen Bilimleri Enstitüsü Dergisi*, vol. 22, no. 2, pp. 397-401, 2018.

[16] B. Yuan, X. Liu, H. Fu, J. Liu, Q. Zhu, and M. Wu, "One-step synthesis of flower-like Cu2O photoelectric materials by hydrothermal method," *Solar Energy*, vol. 188, pp. 265-270, 2019.

[17] M. Claros, I. Gràcia, E. Figueras, and S. Vallejos, "Hydrothermal synthesis and annealing effect on the properties of gas-sensitive copper oxide nanowires," *Chemosensors*, vol. 10, no. 9, 353, 2022.

[18] X. Chen, K. Cui, Z. Hai, W. Kuang, L. Wang, J. Zhang, and X. Tian, "Hydrothermal synthesis of Cu2O with morphology evolution and its effect on visible-light photocatalysis," *Materials Letters*, vol. 297, 129921, 2021.

[19] S. Cao, H. Chen, T. Han, C. Zhao, and L. Peng, "Rose-like Cu2O nanoflowers via hydrothermal synthesis and their gas sensing properties," *Materials Letters*, vol. 80, pp. 135-139, 2016.

[20] L. Grote, S. A. Hussak, L. Albers, K. Stachnik, F. Mancini, M. Seyrich, et al., "Multimodal imaging of cubic Cu2O@ Au nanocage formation via galvanic replacement using X-ray ptychography and nano diffraction," *Scientific Reports*, vol. 13, no. 1, 318, 2023.

[21] H. H. Kadhim, N. Hasan, and A. J. Haider, "Characterization of superconductor materials doped with nanoparticles on their properties," *Journal of Applied Sciences and Nanotechnology*, vol. 2, no. 3, pp. 18-36, 2022.

[22] M. J. Siegfried and K. S. Choi, "Electrochemical crystallization of cuprous oxide with systematic shape evolution," *Advanced Materials*, vol. 16, no. 19, pp. 1743-1746, 2004.

[23] I. Raya, A. Ahmad, A. F. Alkaim, E. R. Alwaily, R. Luque, et al., "Synthesis, characterization and photodegradation studies of copper oxide–graphene nanocomposites," *Coatings*, vol. 11, no. 12, 1452, 2021.

[24] Y. Sui, W. Fu, H. Yang, Y. Zeng, Y. Zhang, Q. Zhao, et al., "Low temperature synthesis of Cu2O crystals: shape evolution and growth mechanism," *Crystal Growth & Design*, vol. 10, no. 1, pp. 99-108, 2010.

[25] L. R. Owen, E. J. Pickering, H. Y. Playford, H. J. Stone, M. G. Tucker, and N. G. Jones, "An assessment of the lattice strain in the CrMnFeCoNi high-entropy alloy," *Acta Materialia*, vol. 122, pp. 11-18, 2017.

[26] A. A. Al-Tabbakh, N. Karatepe, A. B. Al-Zubaidi, A. Benchaabane, and N. B. Mahmood, "Crystallite size and lattice strain of lithiated spinel material for rechargeable battery by X-ray diffraction peak-broadening analysis," *International Journal of Energy Research*, vol. 43, no. 5, pp. 1903-1911, 2019.

[27] S. Kamila and V. Venugopal, "Synthesis and structural analysis of different CuO nanoparticles," *International Journal of Applied Science and Engineering*, vol. 14, no. 3, pp. 133-146, 2017.

[28] S. Ş. Akın, S. K. Kirdeciler, F. Kazanç, and B. Akata, "Critical analysis of zeolite 4A synthesis through one-pot fusion hydrothermal treatment approach for class F fly ash," *Microporous and Mesoporous Materials*, vol. 325, 111338, 2021.

[29] M. Soldemo, J. H. Stenlid, Z. Besharat, M. Ghadami Yazdi, A. Onsten, C. Leygraf, et al., "The surface structure of Cu2O (100)," *The Journal of Physical Chemistry C*, vol. 120, no. 8, pp. 4373-4381, 2016.

[30] Q. Zhang, K. Zhang, D. Xu, G. Yang, H. Huang, F. Nie, et al., "CuO nanostructures: synthesis, characterization, growth mechanisms, fundamental properties, and applications," *Progress in Materials Science*, vol. 60, pp. 208-337, 2014.

[31] J. Xue, W. Liang, X. Liu, Q. Shen, and B. Xu, "Crystallization behavior and formation mechanism of dendrite Cu2O crystals," *CrystEngComm*, vol. 14, no. 23, pp. 8017-8022, 2012.

[32] R. Kara, H. Lahmar, L. Mentar, R. Siab, F. Kadirgan, and A. Azizi, "Electrochemical growth and characterization of

Cu2O: Na/ZnO heterojunctions for solar cells applications," *Journal of Alloys and Compounds*, vol. 817, 152748, 2020.

[33] S. Yadav and P. Bajpai, "Synthesis of copper sulfide nanoparticles: pH dependent phase stabilization," *Nano-Structures & Nano-Objects*, vol. 10, pp. 151-158, 2017.

[34] X. Fuku, M. Modibedi, and M. Mathe, "Green synthesis of Cu/Cu2O/CuO nanostructures and the analysis of their electrochemical properties," *SN Applied Sciences*, vol. 2, pp. 1-15, 2020.

[35] C. H. Kuo, C. H. Chen, and M. H. Huang, "Seed-mediated synthesis of monodispersed Cu2O nanocubes with five different size ranges from 40 to 420 nm," *Advanced Functional Materials*, vol. 17, no. 18, pp. 3773-3780, 2007.

[36] S. B. Aziz, O. G. Abdullah, A. M. Hussein, R. T. Abdulwahid, M. A. Rasheed, H. M. Ahmed, et al., "Optical properties of pure and doped PVA: PEO based solid polymer blend electrolytes: two methods for band gap study," *Journal of Materials Science: Materials in Electronics*, vol. 28, pp. 7473-7479, 2017.

[37] S. Constant, H. L. Wienk, A. E. Frissen, P. de Peinder, R. Boelens, D. S. Van Es, et al., "New insights into the structure and composition of technical lignins: a comparative characterisation study," *Green Chemistry*, vol. 18, no. 9, pp. 2651-2665, 2016.

[38] X. Gong, W. Tian, L. Wang, J. Bai, K. Qiao, and J. Zhao, "Biological regeneration of brewery spent diatomite and its reuse in basic dye and chromium (III) ions removal," *Process Safety and Environmental Protection*, vol. 128, pp. 353-361, 2019.

[39] S. Arya, A. Singh, and R. Kour, "Comparative study of CuO, CuO@Ag and CuO@Ag: La nanoparticles for their photosensing properties," *Materials Research Express*, vol. 6, no. 11, 116313, 2019.

[40] M. R. Olson, M. Victoria Garcia, M. A. Robinson, P. Van Rooy, M. A. Dietenberger, M. Bergin, and J. J. Schauer, "Investigation of black and brown carbon multiple-wavelength-dependent light absorption from biomass and fossil fuel combustion source emissions," *Journal of Geophysical Research: Atmospheres*, vol. 120, no. 13, pp. 6682-6697, 2015.

[41] G. L. Tan, D. Tang, D. Dastan, A. Jafari, J. P. Silva, and X. T. Yin, "Effect of heat treatment on electrical and surface properties of tungsten oxide thin films grown by HFCVD technique," *Materials Science in Semiconductor Processing*, vol. 122, 105506, 2021.

[42] S. Rajamanickam, S. M. Mohammad, and Z. Hassan, "Effect of zinc acetate dihydrate concentration on morphology of ZnO seed layer and ZnO nanorods grown by hydrothermal method," *Colloid and Interface Science Communications*, vol. 38, 100312, 2020.

[43] D. J. Late, P. A. Shaikh, R. Khare, R. V. Kashid, M. Chaudhary, M. A. More, and S. B. Ogale, "Pulsed laser-deposited MoS2 thin films on W and Si: field emission and photoresponse studies," *ACS Applied Materials & Interfaces*, vol. 6, no. 18, pp. 15881-15888, 2014.

[44] L. C. Bourne, P. Y. Yu, A. Zettl, and M. L. Cohen, "High-pressure electrical conductivity measurements in the copper oxides," *Physical Review B*, vol. 40, no. 16, 10973, 1989.

[45] M. M. Ibrahim, M. A. Hassan, and K. I. Hassoon, "Characterization of FeS2 Thin Film Prepared by Spray Pyrolysis Method for Optoelectronic Applications," *Journal of Applied Sciences and Nanotechnology*, vol. 2, no. 3, pp. 78-84, 2022.

[46] R. Schropp and A. Madan, "Properties of conductive zinc oxide films for transparent electrode applications prepared by rf magnetron sputtering," *Journal of Applied Physics*, vol. 66, no. 5, pp. 2027-2031, 1989.

[47] S. Sharma, J. Bijwe, and M. Kumar, "Comparison between nano-and micro-sized copper particles as fillers in NAO friction materials," *Nanomaterials and Nanotechnology*, vol. 3, p. 12, 2013.